Synthesis of metastable phases via pulsed-laser-induced reactive quenching at liquid-solid interfaces

S. B. Ogale, P. P. Patil, D. M. Phase, Y. V. Bhandarkar, S. K. Kulkarni, Smita Kulkarni,
S. V. Ghaisas, and S. M. Kanetkar
Department of Physics, University of Poona, Pune-411 007, India

V. G. Bhide
School of Energy Studies, University of Poona, Pune-411 007, India

Supratik Guha
Department of Materials Science, University of Southern California, Los Angeles, California 90089-0241
(Received 13 January 1987; revised manuscript received 2 September 1987)

High-power pulsed-laser-induced transformations at liquid-solid interfaces are examined with a view to synthesize new metastable phases of materials. Specifically, two types of problems are studied: (1) laser-induced synthesis of compound films at liquid-solid interfaces (called "reactive quenching" because the synthesized compound derives its atomic constituents from the participating liquid and solid systems), and (2) laser-induced alloying of layered structures under a liquid medium whose chemical participation in the process is minimal. The reactive-quenching process has been investigated for three different systems, viz., $Fe:H_2O$, $Fe:NH_3$ (liquid), and $W:C_6H_6$ (benzene), and the results clearly demonstrate that this process can lead to interesting possibilities of synthesis of metastable phases of materials. The identification of metastable compound phases and their microstructural transformations upon subsequent thermal annealing are investigated by using the techniques of conversion-electron Mössbauer spectroscopy, glancing-angle x-ray-diffraction measurements, Rutherford-backscattering spectrometry, x-ray-photoelectron spectroscopy, and transmission-electron microscopy. In the $Fe:H_2O$ and $Fe:NH_3$ cases the as-irradiated state shows the presence of FeO and γ-Fe-N austenite, respectively, while in the $W:C_6H_6$ case a multiphase composite comprised of W_3C, β-W_2C, and WC_{1-x} is observed. Laser-induced alloying of layered structures in the liquid ambient has been studied in the case of the Fe-Al system, and it has been established that processing under liquid nitrogen leads to distinctly different results as compared to laser alloying in air or at liquid-nitrogen temperature in an inert-gas ambient. Time-resolved reflectivity measurements are carried out at the liquid-solid interface to obtain information about the possible mechanisms which could be responsible for the observed effects.

INTRODUCTION

In recent years considerable interest has been shown in the use of directed-energy processing techniques to modify the properties of material surfaces. Among the radiation-processing techniques[1-6] which are being actively applied in the field of material science, the technique of laser treatment has acquired considerable significance during the past few years. An enormous amount of experimental and theoretical work has been done on pulsed and cw laser treatment of materials; however, in most of this work the material systems used have almost invariably been in solid state. Only recently has an interest grown in laser-induced reactions in vapor phase or at vapor-solid interfaces, with a view to synthesize metastable phases of materials.[7,8] This research area, primarily identified as chemical-vapor deposition (CVD), makes use of the pulsed laser beam to induce transient thermochemical or photochemical reactions in vapor phase, leading subsequently to the deposition of reaction products onto an adjacent substrate in the form of elemental, alloy, or compound films. The photochem-

ical aspect of laser-induced reactions has also been profitably utilized in the context of etching applications,[9,10] especially in the field of electronics, wherein the direct writing character of laser beam is of great importance. There have been hardly any attempts, however, to explore the possibility of using pulsed-laser-induced transformations in liquid media or at liquid-solid interfaces to synthesize metastable phases. The objective of this paper is to demonstrate the feasibility of this concept[11-13] via use of a few liquid-solid systems as vehicles for experimentation. Specifically, two types of problems have been studied in this work, viz., (1) laser-induced synthesis of compound thin films wherein the compound derives its atomic constituents partly from liquid and solid systems and (2) laser-induced alloying of layered structures under a liquid medium whose chemical participation in the process in minimal. In the context of laser-induced synthesis of compound films three systems, viz., $Fe:H_2O$, $Fe:NH_3$ (liquid), and $W:C_6H_6$ (benzene) are studied and reported in this paper, while in the context of laser-induced alloying an Fe-Al sandwich structure is studied with liquid nitrogen as an ambient.

The results and discussion have been presented in three sections. The first section concerns the synthesis aspect while the second concerns the alloying concept. The third section contains the discussion about the possible mechanism for the observed quench rate enhancement and the metastable phase formation with reference to the time-resolved reflectivity measurements.

I. SYNTHESIS VIA REACTIVE QUENCHING AT A LIQUID-SOLID INTERFACE

A. Fe:H₂O case

The iron foils used in these experiments were obtained from Goodfellow metals and were 99.999% pure. These foils were appropriately microetched prior to use and then treated with a pulsed ruby laser ($\lambda = 694$ nm, pulse width 30 ns). Five characterization techniques, viz., conversion electron Mössbauer spectroscopy[14] (CEMS), Rutherford-backscattering spectrometry (RBS), x-ray diffraction (normal as well as glancing-angle geometries), x-ray photoelectron spectroscopy (XPS), and transmission electron microscopy (TEM) were used to study the samples. The glancing-angle x-ray patterns were obtained on a Rigaku (Japan) machine by keeping the glancing angle of incidence fixed at 6°. The XPS spectra were recorded on a VG Mark IV system, while the TEM results were obtained on a Philips EM-420 T microscope. The CEMS measurements were performed by using a constant-acceleration Mössbauer setup with ^{57}Co:RH as the γ-ray source. The 7.3-keV K-shell conversion electrons emitted within a distance of less than ~ 0.25 μm below the surface were detected in a continuous gas flow (He + 4% ethanol) proportional detector. To obtain best fit values of hyperfine interaction parameters the spectra were computer fitted by using the standard MOSFIT code.[15]

The specifications of different samples studied are as follows.

(a) Sample 1—virgin iron foil.

(b) Sample 2 and 3—iron foils treated with laser pulses under water at energy densities of 10 J/cm² and 15 J/cm², respectively.

(c) Sample 4—iron foil treated with laser pulses in air at an energy density of 10 J/cm².

In order to enhance the effects, each spot was irradiated twice.

The CEMS results for samples 1, 2, 3, and 4 are shown in Figs. 1(a), 1(b), 1(c), and 1(d), respectively. In analyzing the CEMS data it must be remembered that each CEMS spectrum represents the state of the sample over a depth of ~ 0.25 μm below the surface. The RBS results for samples 1 and 2 are given in Fig. 2, and these help to reveal the modifications occurring over a depth of ~ 1 μm. The x-ray diffraction data for samples 2 and 4, which are of interest from the standpoint of comparison between laser treatment in liquid and air ambients, are given in Fig. 3, while the corresponding XPS results are shown in Fig. 4. The TEM pictures are given in Figs. 5–7.

The CEMS spectrum of Fig. 1(a) shows a single sextet contribution which corresponds to α-Fe (internal magnetic field 330 kOe), while the spectrum of Fig. 1(b) shows two significant quadrupole-split doublets in addition to α-Fe. One of the doublets has an isomer shift (δ_{IS}) of 0.85 mm/sec and quadrupole splitting (Δ_{QS}) of 0.64 mm/sec; while the other doublet has an δ_{IS} of 1.09 mm/sec and Δ_{QS} of 0.65 mm/sec. The two doublets together correspond to the FeO phase; the δ_{IS} values being somewhat higher than the value reported for this phase by Elias and co-workers.[16] The gradation of composition over the 0.25 μm depth scanned by the CEMS tech-

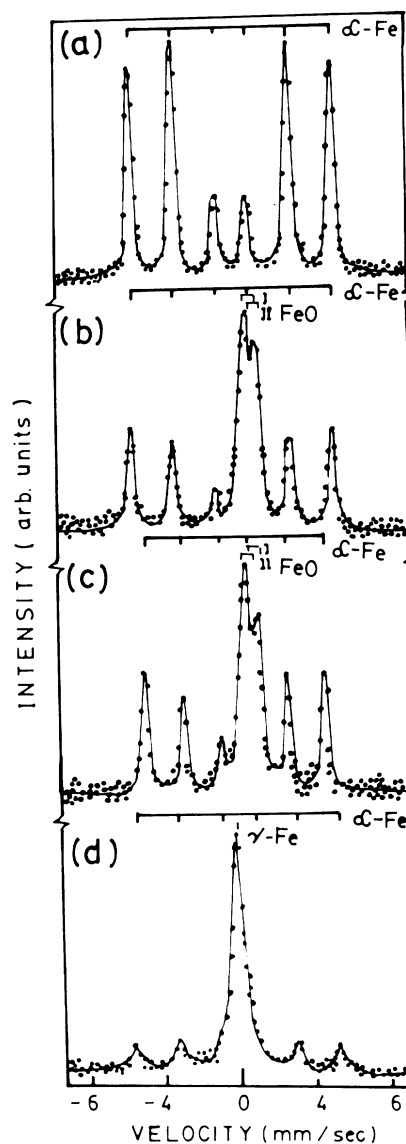
FIG. 1. Room-temperature CEMS spectra of (a) virgin iron foil; (b) iron foil laser treated in H₂O at an energy density of (b) 10 J/cm²; (c) 15 J/cm²; (d) iron foil laser treated in air at energy density of 10 J/cm².
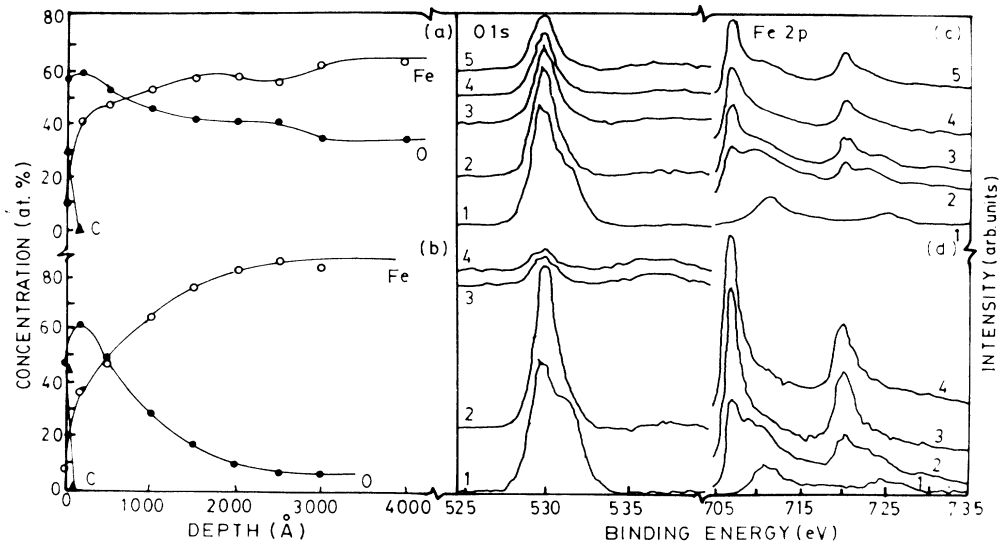
FIG. 2. Rutherford backscattering spectra of virgin iron foil (———) and iron foil laser treated in H_2O at energy density of 10 J/cm^2 (— — —). The spectra were recorded by using 2-MeV He^+ beam.

nique could be responsible for such differences. As the RBS results would indicate, such gradation does exist in the sample. FeO is the most unusual form among the oxides of iron and it can be obtained only by rapid quenching from high temperature.[17] Its presence in our sample brings out the quenching character of the studied process, while its formation from the iron-water system demonstrates the reactive aspect. In order to further justify the formation of this form of iron oxide, we now discuss the RBS, XPS, and XRD data.

The RBS spectra of Fig. 2 reveals that the iron signal is significantly depleted over a depth of ~ 1 μm in the case of sample 2 as compared to the case of sample 1; the depletion being due to the incorporation of oxygen. Since oxygen has considerably lower values of Z and M as compared to iron, its backscattering cross section is also lower by almost a factor of 10, and hence the corresponding signal is weaker. However, the fact that a small but clear step is seen at the location of the oxygen surface signal (marked O) shows that a significant quantity of oxygen is incorporated over a large depth. Computer simulations corresponding to the backscattering experiment bring out that the oxygen incorporated region of sample 2 can be roughly divided into three subregions: (i) A top 1000-Å layer having an oxygen concentration of 50 at. %; (ii) an intermediate thick layer (thickness 4500 Å) having a slowly decaying oxygen concentration with an average composition of 40–45 at. %; and (iii) an underlayer having a thickness of 4000 Å over which the oxygen concentration gradually decays to zero. The RBS result thus supports the CEMS observation of near-stoichiometric FeO in the top layer of sample 2. As may be noticed, the RBS data also gives us information about the oxygen-deficient thick layer in the deeper region, which is inaccessible to the CEMS technique.

The glancing-angle x-ray data given in Fig. 3(a) also shows the presence of FeO in the surface layer (1000 Å thick), and this can be further confirmed from the XPS results shown in Figs. 4(a) and 4(b). The XPS depth profiles show that the concentration of Fe and O are almost comparable to each other in the top 1000-Å layer, and in the thick region below the top layer the concentration is uniformly lower, which is consistent with the RBS data. The chemical states of iron and oxygen can be inferred from the Fe $2p$ and O $1s$ contributions seen

FIG. 3. X-ray diffraction patterns for iron foil laser treated in H_2O [(a) and (b)] and iron foil laser treated in air [(c) and (d)]. The energy density in both cases is 10 J/cm^2. The patterns in (a) and (c) are recorded in glancing-angle geometry, while (b) and (d) are recorded in normal geometry.

FIG. 4. X-ray photoelectron spectroscopy (XPS) results for an iron foil laser treated in H_2O [(a) and (c)] and an iron foil laser treated in air [(b) and (d)]. The "Fe $2p$" and "O $1s$" contributions represented by curves 1, 2, 3, 4, and 5 correspond to chemical states at depths of 0, 500, 2000, 3000, and 4000 Å below the surface.

for different depths subsequent to argon-ion sputtering of the overlayers. The positions of these contributions in all oxides of iron have been studied in great detail by Mills and co-workers;[18] and they point out that the appearance of a satellite peak at an energy of 5 eV above the Fe $2p_{3/2}$ peak is the distinguishing feature of the FeO phase and is absent in the case of other oxides such as Fe_3O_4 and Fe_2O_3. Our spectra clearly show the presence of such a satellite in addition to other aspects discussed by Mills and co-workers[18] in the context of the FeO phase. This proves beyond doubt that we have an FeO phase in the top surface layers. The O $1s$ features in the case of the FeO phase have also been discussed by Mills and co-workers,[18] and our results are in good agreement with these as well. The Fe $2p$ and O $1s$ contributions indicated by lines 3–5 in Fig. 4(c) represent the chemical state of oxygen-deficient FeO coordination, seen in the RBS and XPS depth profiles.

The x-ray diffraction pattern for sample 2 obtained in normal geometry [Fig. 3(b)] allows us to further explore the features of the oxygen-deficient FeO coordination mentioned above; since in this geometry the x rays penetrate deeper. The positions of diffraction lines in Fig. 3(b) can be explained by assuming that contributions of α-Fe and an oxygen-deficient FeO-like coordination having a lattice constant of 4.03 Å coexist in the region explored. On the basis of Vegard's law, applied to α-Fe (lattice constant 2.86 Å) and near-stoichiometric FeO (lattice constant 4.3 Å), one can easily obtain the composition of oxygen-deficient FeO coordination to be $Fe_{55}O_{45}$, which is reasonably consistent with RBS result.

In order to see whether an increase in the laser energy density has a significant influence on the stoichiometry and the basic pattern of observations, we irradiated an iron sample under water at an energy density of 15

J/cm^2. The corresponding CEMS spectrum [Fig. 1(c)] has features similar to those of the spectrum of sample 2 [Fig. 1(b)]; the δ_{IS} (Δ_{QS}) values of the doublets being 0.74 mm/sec (0.72 mm/sec) and 1.06 mm/sec (0.82 mm/sec), which are closer to the values reported by Elias and co-workers.[16] Since an enhanced energy density is expected to enhance the overall process time scale, it could lead to better stoichiometry.

Cross-section transmission electron microscopy studies further substantiate the presence of FeO and α-Fe phases in iron samples treated under water. In order to obtain cross-section TEM pictures the samples were mechanically thinned to about 50 μm and subsequently argon-ion milled to electron transparancy.

The total thickness of the region of laser-induced surface modification was measured to be greater than about 1 μm. The polycrystalline diffraction pattern (Fig. 5) taken from the laser-modified region could be indexed in terms of a mixture of a fcc phase of lattice constant 4.28 Å (FeO) and a bcc phase of lattice constant 2.86 Å (α-Fe). Even when the smallest selected area aperture was used, the measurement did not lead to single-crystal patterns indicating microcrystalline nature of the laser modified region. Two kinds of grains were observed (Fig. 6), a larger variety of average diameter 0.3 μm and a finer globular variety (average diameter 0.017 μm) embedded in it. Measurement of convergent-beam diffraction patterns (CBDP) obtained with a beam spot size of about 400 Å and taken at random regions of Fe-FeO mixture yielded single-crystal patterns with lattice constants of 4.31 and 2.86 Å which correspond to the lattice constants of FeO and α-Fe phases. Figure 7 shows a CBDP which was identified to be from an FeO microcrystallite. Further confirmation of the coexistence of the two phases was brought about from the observa-
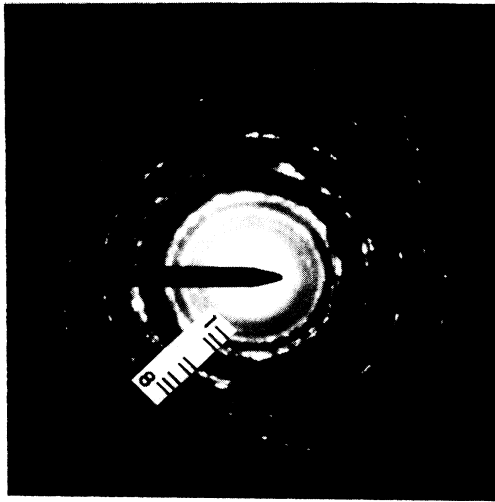
FIG. 5. Polycrystalline diffraction pattern from a typical surface layer region. Labeled rings correspond to different planes as follows: (1) FeO(111), (2) FeO(200), (3) Fe(110), (4) FeO(220), (5) Fe(200), (6) FeO(311), (7) FeO(222), (8) Fe(211).

tion of Moiré fringes in regions of the bright field images. The measured fringe periodicity of 32 Å is in good agreement with the calculated periodicity of 34 Å, where Fe(110) and FeO(200) are the operating reflections.

It is now useful to reveal the differences in the results of processing in liquid and in air, by comparing the states of sample 2 and 4. Surprisingly, the air-treated sample (4) shows a significant contribution of γ-Fe phase[19] (singlet with $\delta_{IS} = -0.001$ mm/sec) in addition to a small contribution of FeO-like phase and a contribution due to α-Fe. The presence of γ-Fe can also be inferred from the x-ray diffraction results of Figs. 3(c) and 3(d). The XPS results for sample 4 [Figs. 4(b) and 4(d)] show that the major quantity of the oxygen incorporated
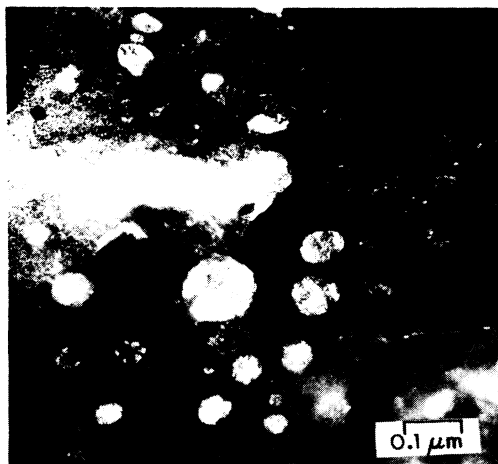
in this sample exists in the surface region up to a depth of 600 Å, and in the thick underlying region only a dilute concentration of oxygen exists. This oxygen could be responsible for stabilizing the γ-Fe phase, which is not known to be stable in the pure form at room temperature except in the form of epitaxial films on fcc substrates.[19] It may be noted that FeO is itself fcc structure, and its formation in distributed regions could help the growth of the fcc phase of iron. The issue of stability of γ-Fe is yet to be fully understood, and its presence in our sample remains an interesting subject to be explored further. Nevertheless, our results presented here clearly bring out that processing in liquid and air ambients lead to characteristically different results.

In order to study the degree of metastability induced into the system, we carried out vacuum annealing of a laser-treated iron foil in H_2O (energy density of 15 J/cm^2) at 300 °C, and 500 °C for 0.5 h in each case. The CEMS spectrum of the sample annealed at 300 °C for 0.5 h [Fig. 8(a)] does not show any major changes, except for small changes in the values of hyperfine-interaction parameters and relative contributions of different spectral components. This spectrum can be computer fitted with the following three contributions.

(i) A doublet: $\delta_{IS} = 1.02$ mm/sec, $\Delta_{QS} = 0.73$ mm/sec.
(ii) A doublet: $\delta_{IS} = 0.72$ mm/sec, $\Delta_{QS} = 0.67$ mm/sec.
(iii) A sextet: $\delta_{IS} = 0.01$ mm/sec, $B_{int} = 331.0$ kOe.

The two quadrupole-split doublets together once again correspond to FeO phase. The sextet is again due to α-Fe. The CEMS spectrum of the sample annealed at 500 °C for 0.5 h is shown in Fig. 8(b). This spectrum is significantly different as compared to the spectrum of Fig. 8(a). The corresponding spectrum can be fitted with two doublets and three sextets, the hyperfine-interaction parameters being as follows.
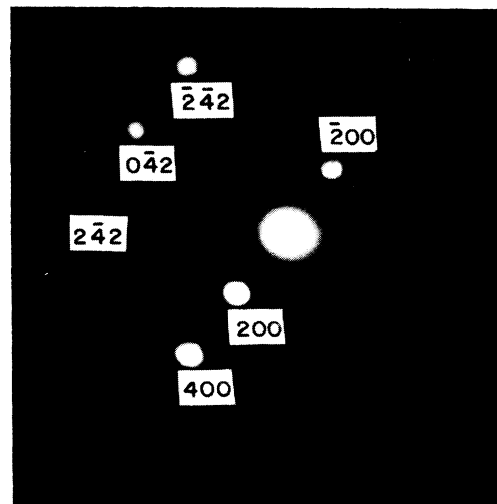

FIG. 6. Centered dark field image using FeO(111), FeO(200), and Fe(110) diffracted beams. Micrograph shows typical grains.

FIG. 7. Convergent beam diffraction pattern (CBDP) from an FeO grain. Beam spot size was approximately 400 Å.

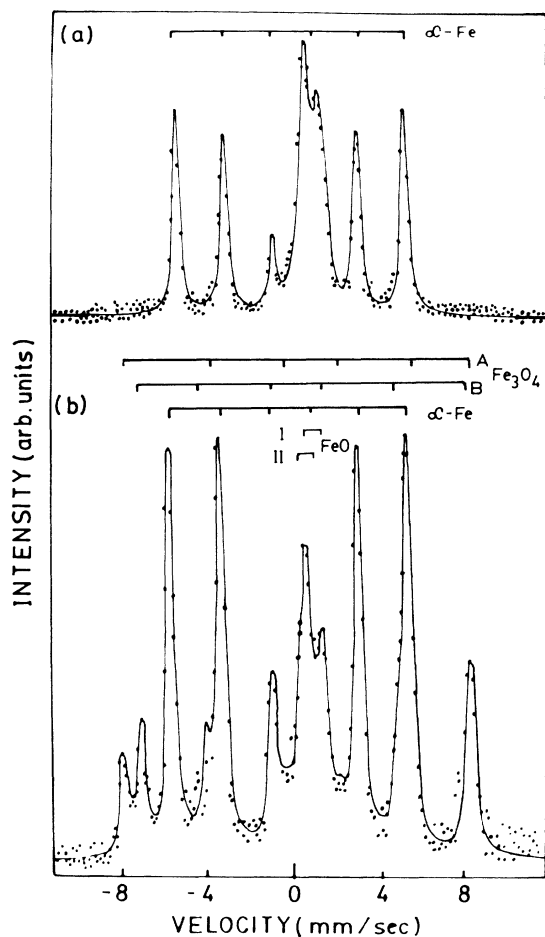FIG. 8. Room-temperature CEMS spectra of iron foil, laser treated in H_2O (15 J/cm^2), annealed at (a) 300°C and (b) 500°C.

(1) A doublet: $\delta_{IS}=1.09$ mm/sec, $\Delta_{QS}=0.80$ mm/sec, contribution equals 8%.

(2) A doublet: $\delta_{IS}=0.78$ mm/sec, $\Delta_{QS}=0.76$ mm/sec, contribution equals 7%.

(3) A sextet: $\delta_{IS}=0.72$ mm/sec, $B_{int}=458$ kOe, contribution equals 11%.

(4) A sextet: $\delta_{IS}=0.24$ mm/sec, $B_{int}=477$ kOe, contribution equals 16%.

(5) A sextet: $\delta_{IS}=-0.01$ mm/sec, $B_{int}=327$ kOe, contribution equals 58%.

The small doublet contribution to the spectrum corresponds to the FeO phase retained after annealing, while the sextet with B_{int} of 327 kOe is due to α-Fe. The appearance of the two sextets with internal magnetic fields of 458 kOe ($\delta_{IS}=0.72$ mm/sec) and 477 kOe ($\delta_{IS}=0.24$ mm/sec) is a clear signature of precipitation of the Fe_3O_4 phase. Thus, the vacuum-annealed sample indicates the partial transformation of FeO into Fe_3O_4,

which is in agreement with the known decomposition process of FeO reported by Greenwood and Howe.[20]

B. Fe:NH₃ case

The experiments reported here were performed by using a pulsed ruby laser (described earlier in the context of the Fe:H_2O case) as well as a XeCl excimer laser ($\lambda=308$ nm, pulse width ~ 25 ns) capable of giving a maximum energy per pulse of 500 mJ. Here we discuss the results of excimer laser treatment to demonstrate that an excimer laser can also be used effectively to achieve compound formation. Although the quantitative details of nitridation with ruby laser are somewhat different, the basic features are still similar, and hence we limit the present discussion only to the excimer laser case. In this case the energy densities up to 3 J/cm^2 could be easily achieved within an acceptable degree of homogeneity by suitable beam guiding and focusing to a spot size of a few mm^2. While processing the samples in liquid ambients, the depth of the liquid covering the sample surface was maintained at 1.5 mm. Pure liquid ammonia was obtained by condensing ammonia vapor on a height-limiting sample pool which was held at a temperature of ~ -60°C during the experiment. Care was taken to flush the sample enclosure with pure dry nitrogen gas while cooling the sample stage, to avoid condensation of water vapor on the sample surface. Subsequently, the ammonia vapor was introduced via a jet directed towards the sample surface. The flow rate of dry nitrogen was gradually reduced to a certain minimum necessary to sweep away the vapors of ammonia formed during laser scanning, which can absorb the uv radiation of the laser beam (photon energy $h\nu=4.03$ eV, N—H bond energy $E=3.3$ eV). The energy density of the laser pulse, spot-to-spot overlap per scan, and the number of scans were varied to study the influence of these parameters on the experimental results. Sample surfaces were chemically etched for cleaning prior to laser treatment. The laser spot was scanned over the sample surface to obtain an effective modified area of 5×5 mm^2.

The CEMS spectrum of the virgin iron foil is shown in Fig. 9(a) and it shows the contribution of α-Fe with an internal magnetic field (B_{int}) value of 330 kOe. The spectrum corresponding to the foil treated at an energy density of 5 J/cm^2 in liquid-NH_3 is shown in Fig. 9(b). This spectrum is significantly different as compared to the spectrum of Fig. 9(a), and it can be computer fitted with the following three contributions.

(i) A sextet: $\delta_{IS}=-0.01$ mm/sec, $B_{int}=330$ kOe.

(ii) A singlet: $\delta_{IS}=-0.02$ mm/sec.

(iii) A doublet: $\delta_{IS}=0.10$ mm/sec, $\Delta_{QS}=0.61$ mm/sec.

The singlet and doublet contributions have been separately shown as an inset in Fig. 9(b) for clarity. The sextet of Fig. 9(b) is once again due to α-Fe, while the singlet and doublet together correspond to the γ-austenite phase of the Fe-N system.[21] This phase is an interstitial
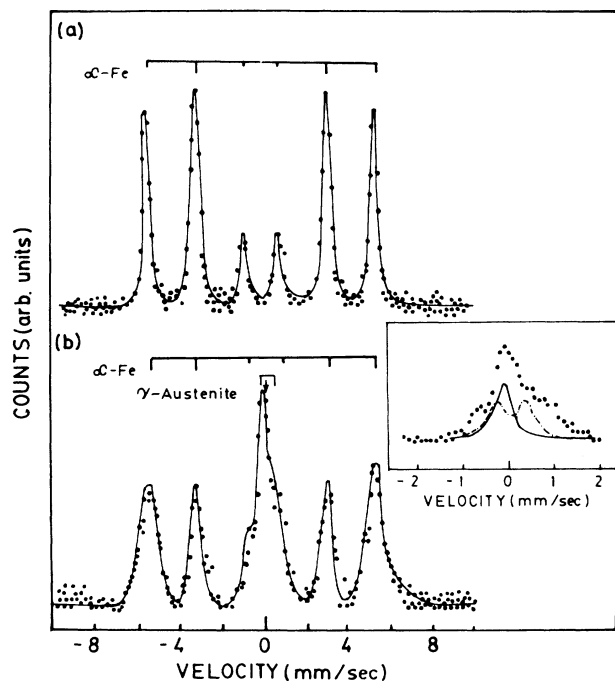
FIG. 9. Room-temperature CEMS spectra of (a) virgin iron foil; (b) iron foil laser treated in liquid NH_3 at an energy density of 5 J/cm^2.

solid solution in which the nitrogen atoms are randomly distributed on octahedral sites. Fe-N austenite having a nitrogen concentration higher than 2.4 wt. % can be retained at room temperature, while below this concentration, a partial transformation to martensite occurs. In our case the concentration is undoubtedly considerably higher than 2.4 wt. %, and better information regarding the concentration can be obtained from quantitative estimates subsequent to phase identification in annealed samples, as will be done later.

In order to confirm the existence of Fe-N austenite in our treated sample, we performed small-angle x-ray diffraction (XRD) measurements. The results are shown in Fig. 10 with (a) representing the untreated and (b) the treated sample. The pattern of Fig. 10(a) shows α-Fe contribution; the line intensity ratios of individual lines being different as compared to the powder data due to presence of texture effects in the foil. The pattern of Fig. 10(b) clearly shows emergence of new lines indicated by arrows, and these lines correspond to the (111), (200), and (220) planes of γ-Fe-N austenite. Thus there is little doubt that this phase is formed in the as-treated sample.

When the laser-treated sample is annealed at the temperature of 250 °C and 350 °C for 0.5 h in each case, the CEMS spectra show systematic changes, as shown in Fig. 11. The spectrum of the sample annealed at 250 °C can be fitted with one singlet and two sextets, the hyperfine-interaction parameters being as follows.

(1) Singlet: $\delta_{IS} = -0.02$ mm/sec.
(2) Sextet: $\delta_{Is} = 0.33$ mm/sec, $B_{int} = 217$ kOe.
(3) Sextet: $\delta_{Is} = 0.01$ mm/sec, $B_{int} = 332$ kOe.

The singlet contribution to the spectrum is now small and it corresponds to the γ-Fe-N austenite retained after annealing. The appearance of the sextet with an internal magnetic field of 217 kOe is a signature of the precipitation of the γ'-Fe$_4$N phase.[21−23] The γ'Fe$_4$N phase has a simple crystal structure, which may be visualized as an fcc iron lattice with nitrogen in the body-center octahedral interstice. In principle, three different internal field values are expected for this phase arising from three different iron sites. One of these is close to the internal field value corresponding to α-Fe, while the remaining two values lie close to 210 kOe and differ only by 1%. Thus in our case the presence of two sextets together should be considered to represent presence of γ'-Fe$_4$N and α-Fe phases. The precipitation of γ'-Fe$_4$N phase in our sample due to thermal annealing can be further justified and confirmed from the CEMS spectrum of the same sample annealed at a higher temperature of 350 °C [Fig. 11(b)]. The CEMS spectrum can now be fitted with three sextets having the following values of hyperfine-interaction parameters.

(1) Sextet: $\delta_{IS} = 0.27$ mm/sec, $B_{int} = 223$ kOe.
(2) Sextet: $\delta_{IS} = -0.01$ mm/sec, $B_{int} = 333$ kOe.
(3) Sextet: $\delta_{IS} = 0.02$ mm/sec, $B_{int} = 348$ kOe.

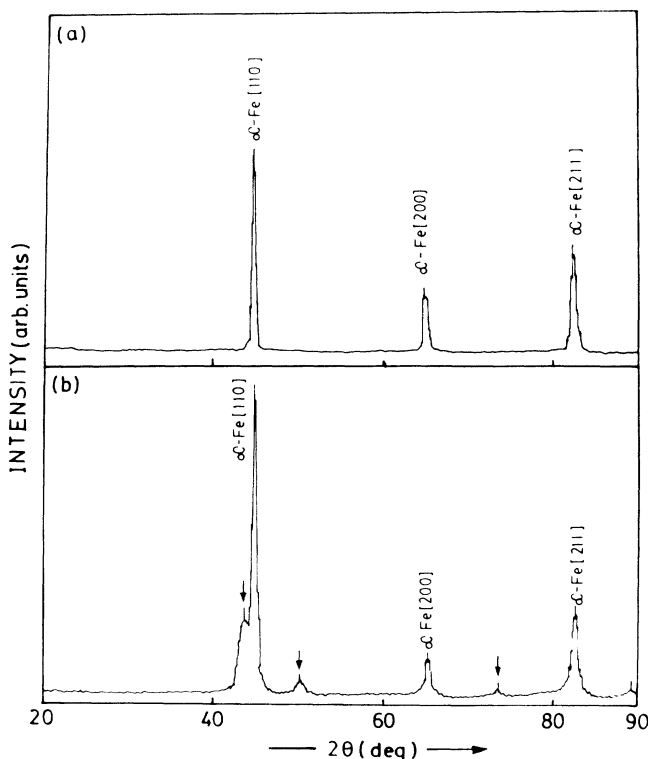The singlet contribution due to γ-Fe-N austenite is absent, indicating that this phase is completely used up in

FIG. 10. The glancing angle x-ray diffraction patterns for (a) virgin iron foil and (b) iron foil laser treated in liquid NH_3 at an energy density of 5 J/cm^2.
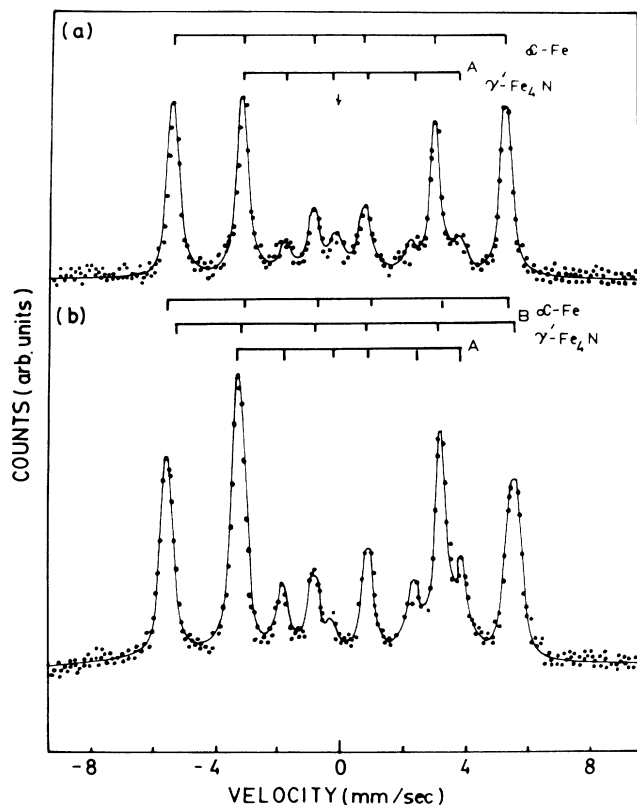
FIG. 11. Room-temperature CEMS spectra of iron foil laser treated in liquid NH_3 at energy density of 5 J/cm^2 and annealed at (a) 250 °C and (b) 350 °C, for 0.5 h in each case.

the solid-state reaction. The relative contributions of the sextets 1, 2, and 3 are 29%, 29%, and 48%, respectively. Clearly, sextets 1 and 3 together represent γ'-Fe$_4$N, while sextet 2 represents unreacted α-Fe. Thus the surface layers of laser-treated and annealed-iron foil contain distributed regions of α-Fe and γ'-Fe$_4$N. In the context of comparison of the present results with those on ion implantation it may be mentioned that implantation at a $N_2{}^+$-ion dose of 10^{17} ions/cm^2 leads to precipitation of α'-martensite and α''-Fe$_{16}$N$_2$ phases[24] which are distinctly different as compared to the phases observed in our case. A systematic study of the dependence of nitridation on laser energy density and different annealing treatments is now in progress.

Finally, it is important to comment on the depth scale of influence due to laser treatment under liquid ammonia. Considering that the conversion electron Mössbauer spectra reveal information from 2500 Å below the surface[14] and that these spectra in the present case show significant modifications subsequent to processing, the depth scale of modification is clearly of the same order. However, in view of the possibility of existence of clusters in the sample, cross-sectional TEM measurements would be required to ensure precise depth-scale characterization.

Our results thus demonstrate that a significant degree of nitridation of iron can be easily achieved if it is treat-

ed with a pulsed excimer laser under liquid ammonia. The as-treated foil has γ-Fe-N austenite phase, which transforms to γ'-Fe$_4$N phase via solid-state reactions with α-Fe upon thermal annealing treatment.

C. W:C$_6$H$_6$ system

In this section we give the results of our experiments on synthesis of carbides, which form another important class of materials which are technologically important. By employing the reactive-quenching process we have been able to synthesize carbides of Fe, Ti, W, etc. using benzene as the liquid ambient. Here we choose to present some results of our work on tungsten carbide with a view to bring out the application of the reactive-quenching process to a noniron based material system.

Tungsten foils (99.9% pure) obtained from Aldrich Chemical Company Inc. (USA) were used in this work. These samples were chemically cleaned with microetchant (sodium hydroxide 10% in distilled water plus potassium ferricynide 30% in distilled water) prior to pulsed ruby laser treatment. These samples were immersed in liquid benzene and were separately treated by laser pulses at energy densities 4.7 J/cm^2 and 6.7 J/cm^2. The x-ray diffraction (XRD) pattern corresponding to virgin tungsten sample is shown in fig. 12(a). This pattern consists of four characteristic lines at 2θ values of 40.20°, 58.20°, 73.20°, 87,0°, representative of W. The line-intensity ratios do not match with the data reported
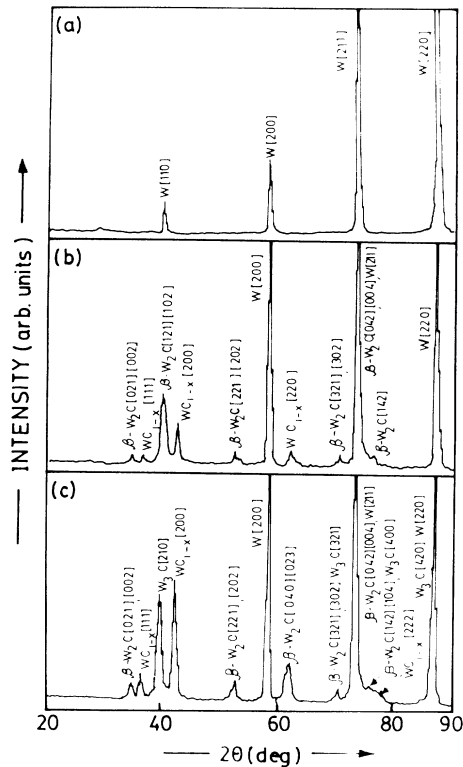

FIG. 12. The glancing angle x-ray diffraction patterns of an untreated tungsten foil (a) and tungsten foils laser treated in liquid C$_6$H$_6$ (benzene) at energy density values of 4.7 J/cm^2 (b) and 6.7 J/cm^2 (c).

for powder samples for obvious reasons, viz., presence of texture effects induced during the synthesis of the foil itself.

The XRD pattern for the sample laser treated in benzene at an energy density of 4.7 J/cm^2 [Fig. 12(b)] exhibits significant changes with reference to the untreated sample. The analysis of different diffraction peaks indicate the formation of β-W$_2$C (hexagonal) and β-WC (WC$_{1-x}$) phases. It is to be noted that all these d values are in close agreement with the reported American Society for Testing Materials (ASTM) (within ± 0.01 Å). The presence of a mixture of phases and texture effect make the quantitative phase analysis difficult; but the identification of the above two phases can be achieved due to their explicit contribution to certain diffraction peaks. For instance, the diffraction peaks at 2θ values 34.60°, 39.50°, 52.30°, 70.00°, 73.10°, and 75.80° indicate β-W$_2$C phase; whereas the peaks at 2θ values 36.40°, 42.50°, and 63.00° clearly reveal the formation of WC$_{1-x}$ phase. The nonstoichiometric WC$_{1-x}$ phase exhibits a defect structure and cannot be retained under normal cooling conditions.[25] Similarly, β-W$_2$C is known to be a typical metastable phase of a W-C system which can result only under very specific conditions of synthesis.

As the energy density is increased to 6.7 J/cm^2, formation of equilibrium W$_3$C phase is observed [Fig. 12(c)]. The emergence of a diffraction line at 2θ value of 40.0° ($d = 2.250$ Å) clearly indicates the presence of this phase along with β-W$_2$C and WC$_{1-x}$. Interestingly enough, the W$_3$C phase with A15-type structure has been reported only recently by Bhat and Holzl[26] and Srivastava et al.[27] The presence of β-W$_2$C, WC$_{1-x}$, and W$_3$C phases in our laser-treated sample establishes the rapid-quenching character of the studied process.

In summary, we have presented here clear evidence that a pulsed laser-induced process at a liquid-solid interface can lead to interesting possibilities for the synthesis of metastable compound films. In order to understand the mechanisms which could play an important role in the reactive quenching, we have carried out "time-resolved reflectivity measurements" at liquid-solid interfaces and the results are discussed in Sec. III.

II. PULSED-LASER-INDUCED ALLOYING IN LIQUID NITROGEN AMBIENT: METASTABLE PHASE FORMATION

In Sec. I we presented examples of pulsed-laser-induced metastable compound formation via transient chemical reactions between liquid and solid systems. In this section we demonstrate that pulsed-laser-induced transformations at liquid-solid interface can also be utilized to achieve interesting alloying effects in layered thin-film structures. In this context one can explore two possibilities: (i) Simultaneous alloying and compound formation, wherein an A-B type layered (or multilayered) thin-film configuration is treated with laser pulses in reactive liquid ambients such as H$_2$O, NH$_3$, or C$_6$H$_6$; or (ii) pulsed-laser treatment of layered thin-film structure under a liquid ambient, which would not have any

significant chemical interaction with the given material systems and will only serve as a medium for rapid heat transport away from the surface layers leading to a possibility of quench-rate enhancement. We have studied the first possibility of "reactive alloying" in different iron-based alloy systems, and these results will be reported separately.[28] More interesting is the second possibility, wherein the liquid overlayer is not expected to pollute the chemistry of the alloying system. During the course of our work we found that liquid nitrogen serves to be one such ambient which has a minimal chemical interaction with a number of material systems, at least at energy densities of less than a few J/cm^2. Since alloying is possible at such energy densities, alloying under liquid nitrogen can be expected to yield new alloying results. We show here that this indeed is the case via use of the Fe:Al and Fe:B systems as a vehicle for experimentation.

In the Fe:Al case samples of aluminum having a thickness of 0.5 mm and purity of 99.99% were used. These samples were annealed and cleaned with mixtures of HF, HCL, HNO$_3$, and double distilled water in a proportion of 1:10:20:69. The substrates were then deposited with a 500-Å-thick overlayer of iron enriched to 30% in the concentration of the ^{57}Fe Mössbauer isotope to enhance the signal-to-noise ratio in the Mössbauer spectra. Without breaking the vacuum, these samples were further coated with a 400-Å-thick layer of aluminum. All depositions were carried out in a Varian ultrahigh-vacuum system. The background pressure was 10^{-10} Torr, and during evaporation it increased to 10^{-7} Torr. The freshly deposited samples were irradiated with ruby laser pulses generated by the JK laser system 2000. The pulse width of this laser beam is 30 ns and the maximum energy output per pulse is ~ 3 J/cm^2. In this investigation two different values of energy density were used, viz. 0.8 J/cm^2 and 1.12 J/cm^2. The irradiations of one set of samples were carried out in air and of another set with the samples submerged in liquid nitrogen, this case being referred in the text as "treatment in liquid-nitrogen ambient." One more set of samples was irradiated by keeping the substrate at liquid-nitrogen temperature; the sample surface region being in an inert-gas atmosphere. Isochronal annealing of the samples treated in liquid-nitrogen ambient was carried out at temperatures of 200, 300, and 400 °C for 1 h in each case to observe the transformation of the structural state. All the Al-Fe-Al samples were characterized by using the technique of conversion-electron Mössbauer spectroscopy (CEMS).

In Fig. 13 are shown the CEMS spectra for an untreated sample (a) and the samples treated in liquid-nitrogen ambient (b), in air (c), and at liquid-nitrogen temperature in an inert-gas ambient (d). The subspectral components are also shown to bring out the differences in modifications imparted to the sample surface due to the differences in the nature of treatments. The component corresponding to α-Fe being consistently present in the CEMS spectra is presented in Figs. 13 and 14; its contribution is not shown explicitly. The spectrum of Fig. 13(a) is a characteristic pattern of the α-Fe phase with an internal magnetic field (B_{int}) of 330 kOe, while
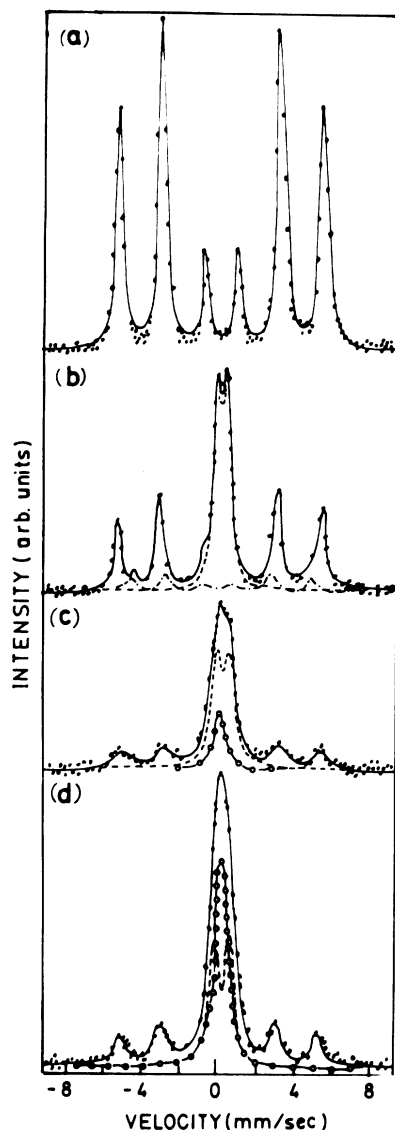
FIG. 13. Room-temperature CEMS spectra of an Al-Fe sample as-deposited (a), laser treated in liquid-nitrogen ambient (b), in air (c), and at liquid-nitrogen temperature in inert atmosphere (d), at an energy density of 1.12 J/cm^2.

the spectrum of Fig. 13(b) shows emergence of a significant contribution near the zero velocity channel at the cost of the contribution of α-Fe. The spectrum of Fig. 13(b) can be fitted with the following subspectral contributions.

(i) Quadrupole doublet: $\delta_{IS}=0.18$ mm/sec, $\Delta_{QS}=0.44$ mm/sec, spectral contribution equals 48%.

(ii) Sextet: $B_{int}=292$ kOe, spectral contribution equals 9%.

(iii) Sextet: $B_{int}=330$ kOe, spectral contribution equals 43%.

The parameters of the doublet are in close agreement

with the values reported for Fe dimers in an aluminum matrix,[29] while the sextet with B_{int} of 292 kOe represents the presence of dilute concentration of Al atoms in the iron matrix. The sextet with B_{int} of 330 kOe is once again due to α-Fe. Iron dimers in an aluminum matrix are a metastable solid solution (MSS) of the Fe-Al system which is known to occur under highly nonequilibrium processing conditions such as under implantation of Fe atoms into an Al matrix.[30] Occurrence of dimeric MSS in our sample treated with a laser in liquid nitrogen establishes the rapid quenching character of the alloying process, though one must resort to a comparison between this case and the case of treatment in air to establish the difference in alloy formation in the two cases. The CEMS spectrum of the sample treated in air is shown in Fig. 13(c), and it can be resolved into the following subspectral components.

(i) Singlet: $\delta_{IS}=0.17$ mm/sec, spectral contribution equals 32%.

(ii) Doublet: $\delta_{IS}=0.18$ mm/sec, $\Delta_{QS}=0.65$ mm/sec, spectral contribution equals 43%.

(iii) Sextet: $B_{int}=326$ kOe, spectral contribution equals 25%.

Firstly, it may be noted that the spectral contribution of α-Fe is significantly less in the air-treatment case as compared to the case of treatment under liquid nitrogen. Secondly, the air-treated sample shows a major contribution of a singlet which is totally absent in the case of treatment under liquid nitrogen. In fact, the singlet and doublet observed in the air-treatment case together correspond to the presence of a Fe_4Al_{13} phase in this sample, with a certain degree of nonstoichiometry reflected by broad linewidths (typically 0.35 mm/sec) and the difference in the singlet-to-doublet contribution ratio with reference to the value for stoichiometric Fe_4Al_{13}. This intermetallic phase is an equilibrium phase of the Fe-Al system, and it has a monoclinic structure with a space group of $C2/m$. It has five characteristic Fe sites which lead to singlet and doublet contributions having hyperfine-interaction parameters in a narrow range of values.[31,32] The Mössbauer spectrum thus appears to be a compounded version of these contributions in the form of one singlet and one doublet, as observed in our case. Presence of vacancies on certain types of sites or departure from stoichiometry in such a structure changes the relative contributions of singlet and doublet. Presence of the nonstoichiometric Fe_4Al_{13} phase (which represents near-equilibrium condition) in the air-treatment case, when compared with the occurrence of dimeric MSS in the case of treatment under liquid nitrogen, establishes that treatment under liquid nitrogen leads to characteristically different alloying effect.

To establish that the structural and chemical state of the sample obtained by treatment under liquid nitrogen is indeed metastable, we annealed the sample treated at an energy density of 1.12 J/cm^2 at temperatures of 200, 300, and 400 °C, for 1 h in each case. Annealing at 200 and 300 °C did not lead to any significant changes in the nature of the CEMS spectrum; however, annealing at
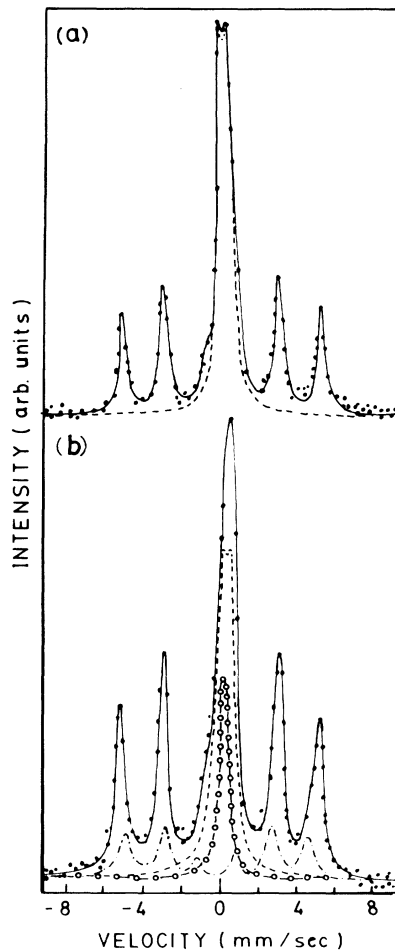
FIG. 14. Room-temperature CEMS spectra of Al-Fe sample, laser treated in liquid-nitrogen ambient at an energy density of 1.12 J/cm² and annealed at (a) 300 °C and (b) 400 °C for 1 h each.

400 °C let to major changes in the spectral characteristics. The spectrum for the case of the sample annealed at 400 °C is shown in Fig. 14(b), and it can be fitted with the following contributions.

(i) Singlet: $\delta_{IS}=0.23$ mm/sec, spectral contribution equals 14%.

(ii) Doublet: $\delta_{IS}=0.23$ mm/sec, $\Delta_{QS}=0.51$ mm/sec, spectral contribution equals 29%.

(iii) Sextet: $B_{int}=294$ kOe, spectral contribution equals 18%.

(iv) Sextet: $B_{int}=322$ kOe, spectral contribution equals 39%.

The singlet and doublet contributions now together correspond to the Fe_4Al_{13} phase with a better stoichiometry. The dimeric MSS which is a high-aluminum solid solution is known to precipitate into the Fe_4Al_{13} phase upon thermal annealing at temperatures of the same order as used here.[30] This establishes the

correctness of our phase identification in the starting state of our sample. It is interesting to point out that annealing of samples treated in air and at liquid-nitrogen temperature in inert ambient at the same temperatures as mentioned above does not lead to any major changes in the features of the corresponding spectra, except for such aspects as narrowing of linewidths and small changes in the relative contributions of singlet and doublet components. This shows that these samples in as-treated state are already near equilibrium.

In another experiment a multilayered structure of a Fe-B system was irradiated with laser pulses under liquid nitrogen to examine the possibility of amorphous phase formation in this glass-forming system using a nanosecond laser. Previously it has been demonstrated that a picosecond laser treatment of such multilayered structure leads to amorphous alloy formation.[33] This sample consisted of alternate layers of Fe and B having thicknesses of 97 and 120 Å, respectively, and the total number of such layers was 21. As in the previous experiments the deposition was carried out under UHV conditions and the layer thicknesses were monitored by an Inficon quartz-crystal monitor. The CEMS spectrum of the as-deposited sample is shown in Fig. 15(a). It shows
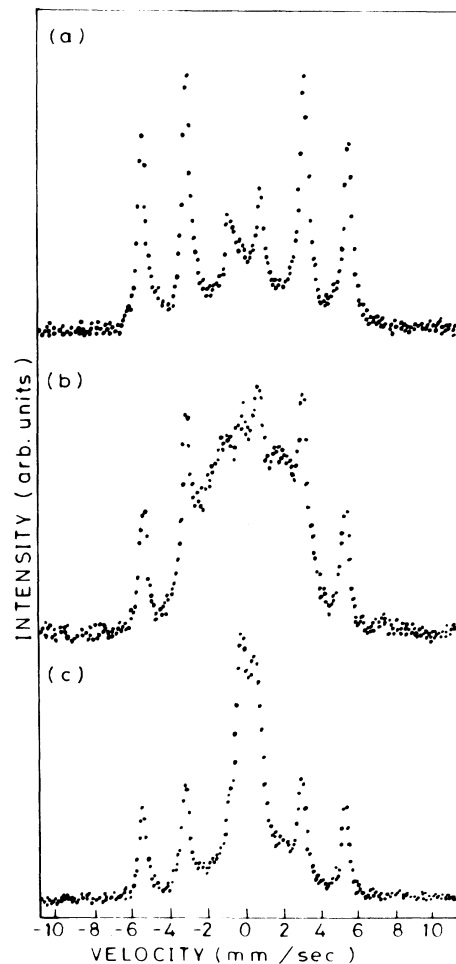

FIG. 15. Room-temperature CEMS spectra of an Fe-B sample as-deposited (a), laser treated in liquid-nitrogen ambient (b), and in air (c) at an energy density of 1.9 J/cm².

the standard hyperfine pattern due to α-Fe. After irradiating this sample under liquid nitrogen with laser pulses having an energy density of 1.9 J/cm^2, the CEMS spectrum of the sample appeared as shown in Fig. 15(b). Clearly, there is a significant degree of disorder introduced into the system. Whether the sample was amorphous or multiphase microcrystalline could not be ascertained. When the as-deposited sample is alloyed in air it leads to the CEMS spectrum shown in Fig. 15(c), which is clearly different as compared to the case represented by the spectrum of Fig. 15(b). The detailed analysis of these phases will be reported separately. [34]

We have thus presented clear evidence that pulsed laser alloying under liquid-nitrogen ambient leads to characteristically and significantly different states of the alloy as compared to the cases of treatment in air or at liquid-nitrogen temperature in an inert ambient. We believe that these findings may have important implications in the broader context of laser alloying of layered thin-film structures.

III. MECHANISM OF TRANSFORMATIONS: TIME-RESOLVED REFLECTIVITY MEASUREMENTS

In order to understand the mechanism of high-power pulsed-laser-induced transformations at liquid-solid interface, time-resolved reflectivity measurements were carried out on the Fe:air and Fe:H$_2$O systems. A 2-mW He-Ne laser beam set at 6° to the normal to the sample surface was employed as a probe beam, while the ruby laser was made incident on the surface at normal incidence. The data were collected using an avalanche photodiode (APD type 30954E) and a Tektronics storage oscilloscope (model 466). These measurements were carried out at various energy densities over a range 1–10 J/cm^2. Representative results corresponding to four values of energy densities are shown in Fig. 16. Heat flow and resolidification kinetics at these energy densities for the Fe:air case are also calculated using a computer code developed by Jain *et al.*,[35] and the corresponding results for the surface layer having a thickness comparable to skin depth are shown in Fig. 17.

First, let us discuss the Fe:air case. At an incident energy density of 1 J/cm^2 it is observed [Fig. 16(a)] that the reflectivity begins to fall at 28.5 ns (t_0) with reference to the registered beginning of pulse-surface interaction and the gradual fall continues over a time duration of 30 ns ($t_1 - t_0$) before a lower stable value of reflectivity is acquired by the surface layer which is probed by the He-Ne beam. Incidently, the thickness of this layer is characteristically represented by the skin depth of iron for a wavelength of 150 Å, and this depth is not more than a few hundred Å. The result of heat-flow calculations for the case of 1 J/cm^2 given by "curve A" of Fig. 17 shows that at this energy density the temperature of the surface layer does not rise above the melting temperature of iron, and thus surface chemical reactions, if any, have to occur in solid phase. Since the drop in reflectivity is of 20–25% and the reflectivity remains at a lower value even though the temperature drops down significantly, it cannot be attributed simply to thermal change in reflectivity. Thus, the drop in
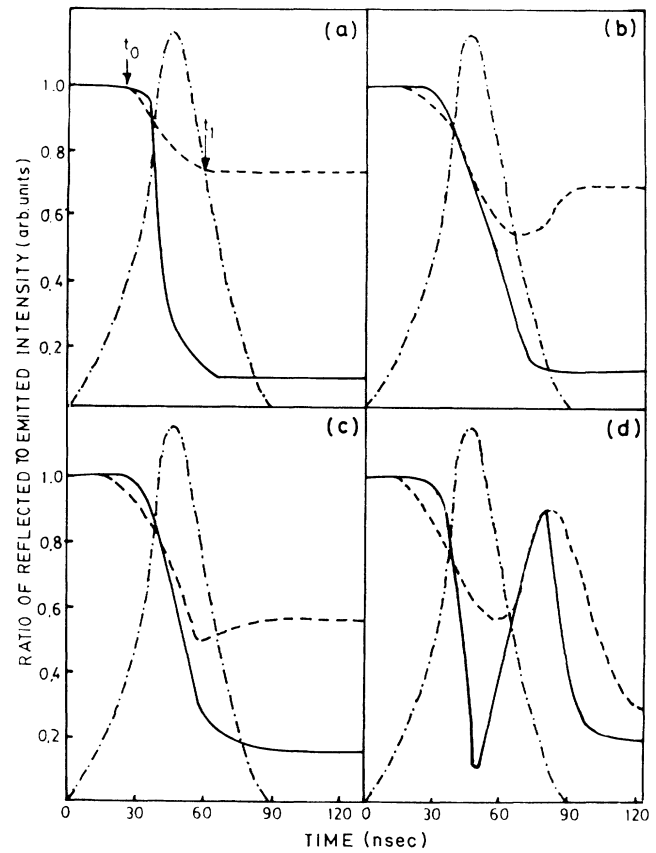

FIG. 16. Reflectivity time profiles for the Fe:air (— — —) and Fe:H$_2$O (———) systems during the irradiation of Ruby pulse (—·—·—·) at energy densities of (a) 1.0 J/cm^2, (b) 1.4 J/cm^2, (c) 1.7 J/cm^2, and (d) 3.4 J/cm^2. t_0: Onset time of the degradation of reflectivity; t_1: terminal point of the degradation of reflectivity.

reflectivity can be attributed to high-temperature oxygen incorporation in the surface layer and associated roughening. If we assume that such processes are brisk at temperatures of 800 °C or more,[36] it can be seen from curve A of Fig. 17 that the temperature of the surface layer rises above 1100 °C at 28 ns following the onset of pulse-surface interaction, and it remains above this temperature over a 32-ns duration. The onset time of reflectivity degradation and duration of the degradation process mentioned earlier are thus in reasonable agreement with the heat-flow calcualtions. At an energy density of 1.4 J/cm^2 [see Fig. 16(b)] the drop in reflectivity is initiated at 18 ns. Further, there is a decrease in reflectivity over a time duration of 42 ns, and then it is increased to a stable value over a duration of 30 ns. The recovery of degraded reflectivity is observed also at the higher value of energy density, viz., 1.7 J/cm^2 [see Fig. 16(c)]. It can be seen from Fig. 16(c) that at this higher value of energy density the onset time of drop in reflectivity is 16.5 ns with reference to the time of initiation of the pulse-surface interaction, and the total duration of reflectivity modification before its stabilization to
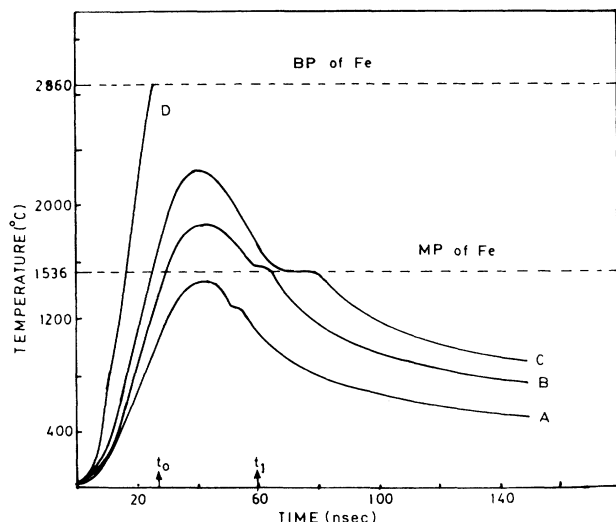
FIG. 17. Computer-simulated temperature-time curves for the Fe:air system irradiated with ruby laser pulse at energy densities (curve A) 1 J/cm^2, (curve B) 1.4 J/cm^2, (curve C) 1.7 J/cm^2, (curve D) 3.4 J/cm^2. The times t_0 and t_1 discussed in the text refer to curve A only. The symbols BP and MP correspond to the boiling and melting point temperatures for iron, respectively.

a specific constant value is 43 ns. Also, it is observed from curves B and C of Fig. 17 that the surface layer of iron melts at both these energy densities of 1.4 and 1.7 J/cm^2. Since diffusion and convection processes are expected to be brisk in the molten state,[37] a rapid degradation of reflectivity is expected in these cases, as is indeed observed. Since turbulence and bubble formation can degrade the reflectivity further, the effective reflectivity should drop significantly during the molten stage, and when the temperature of the surface layer drops below the melting temperature the resolidification is expected to contribute to rise in reflectivity such as the one observed at energy densities of 1.4 J/cm^2 [Fig. 16(b)] and at 1.7 J/cm^2 [Fig. 16(c)]. Also, the values of onset time and time duration are once again reasonably consistent with the corresponding times obtained from reflectivity measurements. However, in these cases the time duration is measured (Fig. 17, curves B and C) between the onset time corresponding to 1100 °C and the time instant at which the resolidification of the melt is just initiated.

In the Fe:H$_2$O case it may be observed that at all three energy densities, viz., 1, 1.4 and 1.7 J/cm^2, the degradation of reflectivity (Fig. 16, continuous curve) begins at a later time as compared to the corresponding results for the Fe:air case (Fig. 16, dashed curve). This establishes that the water overlayer acts as a heat sink at least during the early stages of the process time sequence and does not allow the surface-layer temperature to a value higher than that of a typical reaction temperature. Once the reaction begins, however, the drop in reflectivity is very rapid, demonstrating that significant oxidation of the surface occurs over a very short duration of time. This indeed reflects the reactive-quenching character of the process. We have carried out prelimi-

nary heat-flow calculations for the Fe:H$_2$O system by assuming a convective heat loss to the water overlayer, and these calculations indicate that rapid quenching of reactions should occur in the Fe:H$_2$O case. We do not present these results, however, since a detailed calculation must account for mass transport in fluid state, chemical reactions at high pressure and temperature, etc. This has not yet been done.

In addition to the features discussed earlier there is yet another interesting feature observed at an energy density of 3.4 J/cm^2 [Fig. 16(d)]. Here, in the Fe:air case one can clearly see a sudden rise in the intensity picked up by the APD at a time of 60 ns with reference to the pulse-surface interaction initiation time followed by a drop over a time duration of 33 ns. A similar feature was also observed in the Fe:H$_2$O case, except for the fact that the fall in the reflectivity was much faster in this case. It was also observed that this feature appeared even without the probe beam. Hence it was attributed to emission by the beam-induced surface plasma. It is interesting to observe that in the Fe:H$_2$O case the plasma is quenched almost 2 times faster than the Fe:air case. Plasma quenching is faster at higher pressure due to reduction in the mean free path for recombination events. Thus it is clear that in the Fe:H$_2$O case locally a high-pressure plasma is created and the chemical reactions occur in this phase, leading finally to redeposition of the reaction products on the surface via rerandomization of atomic and molecular trajectories. Similar plasma-quenching processes were also observed at higher energy densities in the Fe:H$_2$O case. Since the energy densities employed for reactive synthesis in the case of the Fe:H$_2$O system (see results of Fig. 1) are comparable or higher than the energy density of 3.4 J/cm^2, we propose that the reactive-quenching process at higher-energy densities occurs in high-pressure plasma phase in addition to the initial reactions in the solid state and molten state.

CONCLUSIONS

Pulsed-laser-induced "reactive quenching" at the interface between a liquid-solid can lead to synthesis of metastable compound phases which derive their atomic constituents from the participating liquid and solid systems. Alloying of layered structures (comprised of elemental constituents which are passive to chemical reaction with nitrogen) under liquid nitrogen can lead to a metastable state of the alloy which is characteristically different from the state obtained by pulsed laser alloying in air or at liquid-nitrogen temperature in an inert-gas ambient. Time-resolved reflectivity measurements are carried out to obtain the information about the mechanisms of transformations. Apart from reactions in the solid state and the molten state, the occurrence of a high-pressure plasma phase is thought to be responsible for the observed reactive-quenching nature of the process.

ACKNOWLEDGMENT

[1]*Laser and Electron Beam Solid Interactions and Material Processing,* Materials Research Society Symposium Proceedings, edited by J. F. Gibbons, L. D. Hess, and T. W. Sigmon (North-Holland, New York, 1981), Vol. 1.

[2]*Laser Processing and Diagnostics,* edited by D. Bauerle (Springer-Verlag, Berlin, 1984).

[3]J. W. Mayer and S. S. Lau, in *Surface Modification and Alloying by Laser, Ion and Electron Beams,* edited by J. M. Poate, G. Foti, and D. C. Jacobson (Plenum, New York, 1981).

[4]V. P. Godbole, S. M. Chaudhari, S. V. Ghaisas, S. M. Kanetkar, S. B. Ogale, and V. G. Bhide, Phys. Rev. B **31**, 5703 (1985).

[5]S. B. Ogale, D. M. Phase, S. M. Chaudhari, S. V. Ghaisas, S. M. Kanetkar, P. P. Patil, V. G. Bhide, and S. K. Date, Phys. Rev. B **35**, 1593 (1987).

[6]S. B. Ogale, Rekha Joshee, V. P. Godbole, S. M. Kanetkar, and V. G. Bhide, J. Appl. Phys. **57**, 2915 (1985).

[7]H. M. Branz, S. Fan, J. H. Flint, B. J. Fiske, Q. Adler, and J. S. Haggerty, Appl. Phys. Lett. **48**, 2 (1986).

[8]R. B. Jackman, J. S. Foard, A. E. Adams, and M. L. Lloyd, J. Appl. Phys. **59**, 6 (1986).

[9]F. A. Houle, in Laser Assisted Deposition, Etching and Doping, edited by S. D. Allen [Proc. Soc. Photo-Opt. Instrum. Eng. **459**, 110 (1984)].

[10]G. L. Loper and M. D. Tabat, J. Appl. Phys. **58**, 3649 (1985).

[11]S. B. Ogale, P. P. Patil, D. M. Phase, S. A. Kulkarni, S. V. Ghaisas, and V. G. Bhide, Materials Research Society Symposium on Beam-Solid Interactions and Transient Processes, Boston, 1986 (unpublished).

[12]P. P. Patil, D. M. Phase, S. A. Kulkarni, s. V. Ghaisas, S. K. Kulkarni, S. M. Kanetkar, and S. B. Ogale, Phys. Rev. Lett. **58**, 238 (1987).

[13]S. B. Ogale, A. Polman, F. O. P. Quentin, S. Roorda, and F. W. Saris, Appl. Phys. Lett. **50**, 138 (1987).

[14]B. D. Sawicka and J. A. Sawicki, in *Mössbauer Spectroscopy—II,* Vol. XXV of *Topics in Current Physics,* edited by U. Gonser (Springer-Verlag, Berlin, 1981).

[15]This MOSFIT program was originally written by E. Kreber from Universite des Saarlands, Saarbruken and it was adopted for ICL 1904S computer by Dr. S. K. Date from National Chemical Laboratory, Pune, India.

[16]D. J. Elias and J. W. Linnet, Trans. Faraday Soc. **65**, 2673 (1969).

[17]N. N. Greenwood and T. C. Gibb, *Mössbauer Spectroscopy* (Chapman and Hall, London, 1971), p. 248.

[18]P. Mills and J. L. Sullivan, J. Phys. D **16**, 723 (1983).

[19]U. Gonser and M. Ron, in *Applications of Mössbauer Spectroscopy,* edited by R. L. Cohen (Academic, New York, 1980), Vol. II, pp. 282–324.

[20]N. N. Greenwood and A. T. Howe, J. Chem. Soc. Dalton 116 (1972).

[21]M. Ron, in *Applications of Mössbauer Spectroscopy,* edited by R. L. Cohen (Academic, New York, 1980), Vol. II, pp. 329–392.

[22]J. Bainbridge, D. A. Channing, W. H. Whitlow, and R. E. Pendlebury, J. Phys. Chem. Solids **34**, 1579 (1973).

[23]G. Longworth and N. E. W. Hartley, Thin Solid Films **48**, 95 (1978).

[24]N. Moncoffre, G. Hollinger, H. Jaffrezic, G. Marest, and J. Tousset, Nucl. Instrum. Methods B **7/8**, 177 (1985).

[25]*The Refractory Carbides,* edited by E. K. Storms (Academic, New York, 1967), p. 143.

[26]Deepak G. Bhat and Robert A. Holzl, Thin Solid Films **95**, 105 (1982).

[27]P. K. Srivastava, T. V. Rao, V. D. Vankar, and K. L. Chopra, J. Vac. Sci. Technol. A **2**, 1261 (1984).

[28]S. B. Ogale, Sushma Joshi, S. M. Kanetkar, S. V. Ghaisas, and V. G. Bhide (unpublished).

[29]S. Nasu, U. Gonser, P. H. Shingu, and Y. Murakami, J. Phys. F **4**, L24 (1974).

[30]B. D. Sawicka, M. Drwiega, J. A. Sawicki, and J. Stanek, Hyp. Int. **4**, 147 (1978).

[31]R. S. Preston and R. Gerlach, Phys. Rev. B **3**, 1519 (1970).

[32]S. Nasu, U. Gonser, and R. S. Preston, J. Phys. (Paris) Colloq. **41**, C1-385 (1980).

[33]C. J. Lin and F. Spaepen, Appl. Phys. Lett. **41**, 721 (1982).

[34]P. P. Patil and S. B. Ogale (unpublished).

[35]A. K. Jain, V. N. Kulkarni, and D. K. Sood, Appl. Phys. **25**, 127 (1981).

[36]R. C. Weast and M. J. Astle, *Handbook of Chemistry and Physics,* 63rd Ed. (CRC, Boca Roton, 1982-83).

[37]M. Berti, L. F. Dona Dalle Rose, A. V. Drigo, C. Cohen, J. Siejka, G. G. Bentini, and E. Jannitti, Phys. Rev. B **34**, 2346 (1986).
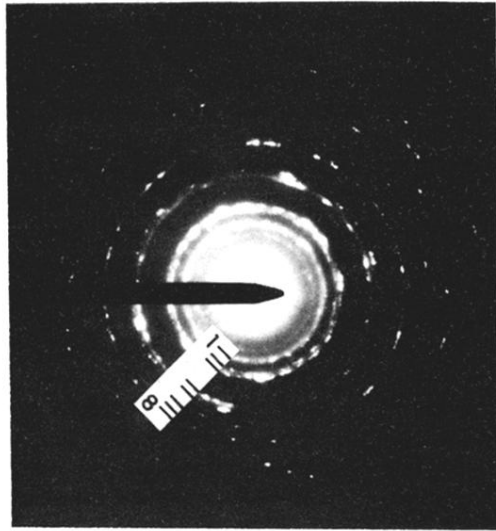
FIG. 5. Polycrystalline diffraction pattern from a typical surface layer region. Labeled rings correspond to different planes as follows: (1) FeO(111), (2) FeO(200), (3) Fe(110), (4) FeO(220), (5) Fe(200), (6) FeO(311), (7) FeO(222), (8) Fe(211).
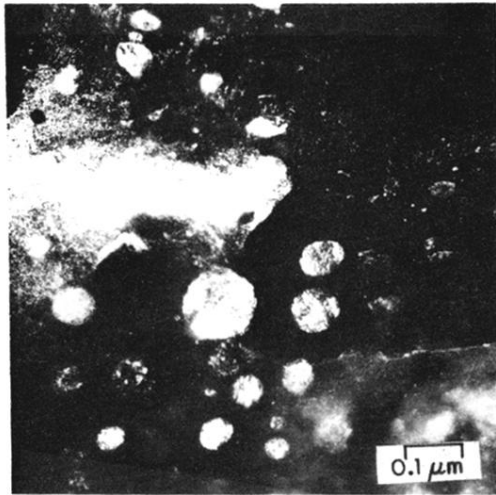
FIG. 6. Centered dark field image using FeO(111), FeO(200), and Fe(110) diffracted beams. Micrograph shows typical grains.
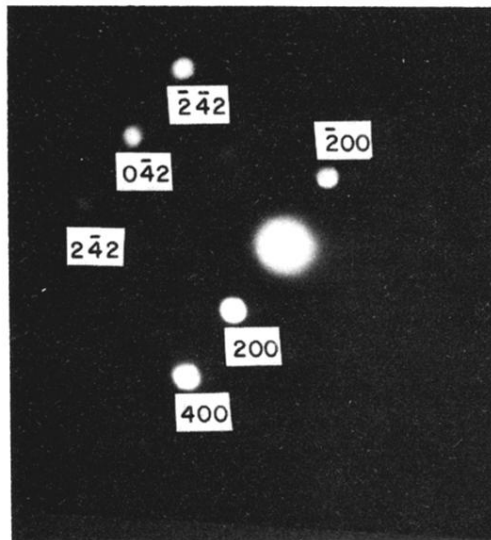
FIG. 7. Convergent beam diffraction pattern (CBDP) from
an FeO grain. Beam spot size was approximately 400 Å.